British Journal of Pharmacology

DOI:10.1111/bph.13019
www.brjpharmacol.org

RESEARCH PAPER

Differential sensitivity of TREK-1, TREK-2 and TRAAK background potassium channels to the polycationic dye ruthenium red

G Braun, M Lengyel, P Enyedi and G Czirják

Department of Physiology, Semmelweis University, Budapest, Hungary

Correspondence
Gábor Czirják, Department of Physiology, Semmelweis University, P. O. Box 259, H-1444 Budapest, Hungary. E-mail: czirjak.gabor@med.semmelweis-univ.hu

Received
18 June 2014
Revised
15 October 2014
Accepted
11 November 2014

BACKGROUND AND PURPOSE

Pharmacological separation of the background potassium currents of closely related K_{2P} channels is a challenging problem. We previously demonstrated that ruthenium red (RR) inhibits TASK-3 ($K_{2P}9.1$), but not TASK-1 ($K_{2P}3.1$) channels. RR has been extensively used to distinguish between TASK currents in native cells. In the present study, we systematically investigate the RR sensitivity of a more comprehensive set of K_{2P} channels.

EXPERIMENTAL APPROACH

K^+ currents were measured by two-electrode voltage clamp in *Xenopus* oocytes and by whole-cell patch clamp in mouse dorsal root ganglion (DRG) neurons.

KEY RESULTS

RR differentiates between two closely related members of the TREK subfamily. TREK-2 ($K_{2P}10.1$) proved to be highly sensitive to RR (IC_{50} = 0.2 μM), whereas TREK-1 ($K_{2P}2.1$) was not affected by the compound. We identified aspartate 135 (D135) as the target of the inhibitor in mouse TREK-2c. D135 lines the wall of the extracellular ion pathway (EIP), a tunnel structure through the extracellular cap characteristic for K_{2P} channels. TREK-1 contains isoleucine in the corresponding position. The mutation of this isoleucine (I110D) rendered TREK-1 sensitive to RR. The third member of the TREK subfamily, TRAAK ($K_{2P}4.1$) was more potently inhibited by ruthenium violet, a contaminant in some RR preparations, than by RR. DRG neurons predominantly express TREK-2 and RR-resistant TREK-1 and TRESK ($K_{2P}18.1$) background K^+ channels. We detected the RR-sensitive leak K^+ current component in DRG neurons.

CONCLUSIONS AND IMPLICATIONS

We propose that RR may be useful for distinguishing TREK-2 ($K_{2P}10.1$) from TREK-1 ($K_{2P}2.1$) and other RR-resistant K_{2P} channels in native cells.

Abbreviations

DRG, dorsal root ganglion; K_{2P}, two-pore-domain K^+ (channel); RR, ruthenium red; RV, ruthenium violet; TALK, TWIK-related alkaline-activated K^+ channel; TASK ($K_{2P}3.1$), TWIK-related acid-sensitive K^+ channel; THIK, TWIK-related halothane-inhibited K^+ channel; TRAAK ($K_{2P}4.1$), TWIK-related arachidonic acid-activated K^+ channel; TREK, TWIK-related K^+ channel; TRESK, TWIK-related spinal cord K^+ channel; TWIK, tandem of pore domains in a weakly inwardly rectifying K^+ channel

Tables of Links

TARGETS		
TALK-1 (K_{2P}16.1)	THIK-1 (K_{2P}13.1)	TRESK (K_{2P} 18.1)
TALK-2 (K_{2P}17.1)	THIK-2 (K_{2P}12.1)	TWIK-1 (K_{2P} 1.1)
TASK-1 (K_{2P}3.1)	TRAAK (K_{2P} 4.1)	TWIK-2 (K_{2P} 6.1)
TASK-2 (K_{2P}5.1)	TREK-1 (K_{2P} 2.1)	
TASK-3 (K_{2P}9.1)	TREK-2 (K_{2P} 10.1)	

LIGANDS
Ruthenium red (RR)

These Tables list key protein targets and ligands in this article which are hyperlinked to corresponding entries in http://www.guidetopharmacology.org, the common portal for data from the IUPHAR/BPS Guide to PHARMACOLOGY (Pawson *et al.*, 2014) and are permanently archived in the Concise Guide to PHARMACOLOGY 2013/14 (Alexander *et al.*, 2013).

Introduction

Different members of the two-pore-domain K^+ channel (K_{2P}) family show characteristic expression patterns, are regulated by extraordinarily diverse mechanisms and contribute to a great variety of physiological processes (Enyedi and Czirják, 2010). These channels give rise to similar macroscopic background (leak) potassium currents, and thus, it is a challenge to distinguish them in whole-cell measurements. Identification of individual K_{2P} channel types is also of importance because the different members of the family may prove to be therapeutic targets in distinct pathophysiological states (Mathie and Veale, 2007; Bittner *et al.*, 2010). Pharmacological properties of K_{2P} channels have been extensively investigated; however, the background K^+ currents were typically affected by relatively non-specific compounds (Lotshaw, 2007). It appears to be difficult to identify highly selective inhibitors of K_{2P} channels, perhaps because of the distinctive structural element, the extracellular cap, which covers the entrance of the ion-conducting pore, and restricts the access of high molecular weight inhibitors to the opening (Brohawn *et al.*, 2012; Miller and Long, 2012).

We previously demonstrated that low micromolar concentrations of ruthenium red (RR) ($[(NH_3)_5Ru\text{-}O\text{-}Ru(NH_3)_4\text{-}O\text{-}Ru(NH_3)_5]Cl_6$) inhibit TASK-3 ($K_{2P}$9.1) background K^+ channels, whereas TASK-1 (K_{2P}3.1) is not affected by the polycationic dye (Czirják and Enyedi, 2003). This observation proved to be useful because of the remarkably selective action of RR distinguishing between the two closely related TASK channels, and despite the limited overall specificity of the compound. RR is known to inhibit a multitude of target proteins, most of them related to the transport or binding of Ca^{2+} (e.g. calcium channels and pumps, as detailed in the Discussion section of Czirják and Enyedi, 2003). A negatively charged amino acid, glutamate 70 (E70) was established as the major determinant of TASK-3 inhibition by RR (Czirják and Enyedi, 2003; Musset *et al.*, 2006; Gonzalez *et al.*, 2013). TASK-1 contains a positive lysine in the corresponding position, and the channel was rendered RR-sensitive by the K70E mutation, indicating that the high charge density ruthenium compound differentiated between the channels by electrostatic interaction on the basis of a single distinct amino acid residue.

Differential sensitivity of TASK-1 and TASK-3 to RR has been extensively used to investigate TASK currents in adrenal glomerulosa cells (Czirják and Enyedi, 2002b), carotid body glomus cells (Kim *et al.*, 2009), cardiomyocytes (Putzke *et al.*, 2007), pulmonary artery smooth muscle cells (Olschewski *et al.*, 2006), motoneurons (Berg *et al.*, 2004; Larkman and Perkins, 2005), cerebellar granule neurons (Lauritzen *et al.*, 2003; Kang *et al.*, 2004; Aller *et al.*, 2005), thalamocortical relay neurons (Musset *et al.*, 2006) and several other cell types (Berg and Bayliss, 2007; Deng and Lei, 2008; Weber *et al.*, 2008; Ernest *et al.*, 2010). We reported previously that in addition to TASK-3, another K_{2P} channel, TWIK-related arachidonic acid-activated K^+ channel (TRAAK; K_{2P}4.1), a member of the TREK subfamily, is also sensitive to RR. Whereas in the case of TASK-3 the Hill coefficient of about 1 was in good accordance with the binding of one RR molecule simultaneously to both E70 residues in the dimer of the subunits, the inhibition of TRAAK by RR was characterized by a Hill coefficient of 2, suggesting that RR inhibits TRAAK and TASK-3 by different mechanisms (Czirják and Enyedi, 2002a).

In the present study, we investigated a more comprehensive set of K_{2P} channels in order to categorize them into RR-sensitive and RR-resistant groups, and also examined the mechanism of action of the inhibitor.

Methods

Plasmids and reagents

The cloning of mouse TASK-1/2/3 (K_{2P}3.1/K_{2P}5.1/K_{2P}9.1), TREK-2 (K_{2P}10.1), TALK-1 (K_{2P}16.1), THIK-1 (K_{2P}13.1) and human and mouse TRESK (K_{2P}18.1) has been described previously (Czirják *et al.*, 2004; Czirják and Enyedi, 2006). Human and mouse TRAAK (K_{2P}4.1) and TREK-1 (K_{2P}2.1), and human TREK-2 channel plasmids were kindly provided by Professor M. Lazdunski and Dr F. Lesage. Drug target nomenclature conforms with British Journal of Pharmacology's Concise Guide to Pharmacology (Alexander *et al.*, 2013). Different mutant versions of these channels were produced with QuikChange site-directed mutagenesis kit (Stratagene, La Jolla, CA, USA) according to the manufacturer's instructions. For the construction of tandem wt/wt, wt/mutant and mutant/wt mTREK-2 channels, the TAA stop codon of the

upstream subunit and the ATG start codon of the downstream subunit were replaced with a unique MunI restriction enzyme site. This introduced a two amino acid linker (glutamine and leucine) between the coding sequences of the concatenated subunits.

Chemicals of analytical grade were purchased from Sigma (St. Louis, MO, USA), Fluka (Milwaukee, WI, USA) or Merck (Whitehouse Station, NJ, USA). Enzymes and kits for molecular biology applications were purchased from Ambion (Austin, TX, USA), Thermo Scientific (Waltham, MA, USA), New England Biolabs (Beverly, MA, USA) and Stratagene.

Purification of ruthenium violet (RV)

RR and RV were dissolved in 0.1 M ammonium acetate (AA) as 10 mM stock solutions, and diluted further in high [K^+] solution before the measurement. In order to purify RV, we applied cation exchange chromatography using carboxymethyl (CM) cellulose resin (Whatman CM52). Crude RR preparation (70 mg) was dissolved in AA (10 mM, 30 mL). The solution was applied to a 1 mL CM cellulose column at a flow rate of 0.4 mL·min^{-1}. The flowthrough was colourless, whereas the column became dark with the adsorbed dyes. Bulk RR was eluted by two rounds of isocratic elution (750 mM AA, 10 mL), followed by washing steps (50 mM AA, 20 mL). Subsequently, RV was eluted with a linear gradient of AA (from 50 mM to 1.5 M, in 20 mL); the major RV peak appeared between 1.2 and 1.4 M. Fractions containing RV were lyophilized, immediately dissolved in 10 mM AA, and stored at –20°C. The calculated molar ratio of RV/RR was increased from 0.1 to 9.5 by the purification. [RV concentration was calculated using the extinction coefficient $\varepsilon = 311$ (g·100 mL^{-1})$^{-1}$·cm^{-1} at 734 nm (Luft, 1971), and molecular weight 751.43 g·mol^{-1} (Hall and Griffith, 1980)].

Animals, Xenopus *oocyte microinjection, isolation of dorsal root ganglion (DRG) neurons*

DRG neurons were derived from six Naval Medical Research Institute mice, purchased from Toxicoop, Budapest, Hungary. Mice were maintained on a 12 h light/dark cycle with free access to food and water. Animals were killed by CO_2 exposure. *Xenopus* oocytes were prepared, the cRNA was synthesized and microinjected as previously described (Czirják *et al.*, 2004) (For the expression of the different channel types, 57 pg – 2.3 ng per oocyte cRNA was injected.). Fifteen frogs were used for the experiments. The animals were maintained in two 50 L tanks, with continuous filtering and water circulation through aquarium pumps at 19°C in an air conditioned room. The frogs were anaesthetized with 0.1% tricaine solution and killed by decerebration and pithing. All treatments of the animals were conducted in accordance with state laws and institutional regulations. The experiments were approved by the Animal Care and Ethics Committee of Semmelweis University (approval ID: XIV-I-001/2154-4/2012). All studies involving animals are reported in accordance with the ARRIVE guidelines for reporting experiments involving animals (Kilkenny *et al.*, 2010; McGrath *et al.*, 2010).

DRGs were dissected from thoracic and lumbar levels of the spinal cord of 40–70-day-old mice. DRGs were collected in sterile PBS (137 mM NaCl, 2.7 mM KCl, 10 mM NaH_2PO_4, pH 7.4 with NaOH) at 4°C. Ganglia were incubated with gentle shaking for 30 min at 37°C in PBS containing 2 mg·mL^{-1} collagenase (type I; Worthington, Lakewood, NJ, USA). Then DMEM-F-12 containing 10% FBS (Lonza, Basel, Switzerland) and 100 U·mL^{-1} penicillin-streptomycin (Sigma) was added, and gentle trituration was performed with a cut 1 mL plastic pipette tip for 10–15 times. Cells were centrifuged at 200× *g* for 5 min, washed three times with culture medium, and plated on plastic culture dishes treated with poly-L-lysine. They were incubated in 95% air – 5% CO_2 mixture at 37°C, and measured after 1–3 days.

Two-electrode voltage clamp and patch clamp measurements

Two-electrode voltage clamp experiments were performed 3 or 4 days after the microinjection of cRNA, as previously described (Czirják *et al.*, 2004). Low [K^+] solution contained (in mM): NaCl 95.4, KCl 2, $CaCl_2$ 1.8, HEPES 5 (pH 7.5 adjusted with NaOH). High [K^+] solution contained 80 mM K^+ (78 mM Na^+ of the low [K^+] solution was replaced with K^+). Background K^+ currents were measured at the end of 300 ms long voltage steps to –100 mV applied every 4 s.

Responses of DRG neurons were measured by whole-cell patch clamp at 37°C. The low [K^+] extracellular solution contained (in mM): NaCl 140, KCl 2, $MgCl_2$ 0.5, $CaCl_2$ 2, glucose 11, HEPES 10, pH 7.4 (adjusted with NaOH). High [K^+] extracellular solution contained 30 mM K^+ (28 mM Na^+ of the low [K^+] solution was replaced with K^+). Pipettes were pulled from borosilicate glass by a P-87 puller (Sutter Instrument Co., Novato, CA, USA) and fire polished. Pipette resistance ranged between 3 and 9 MΩ when filled with the intracellular solution containing (in mM): KCl 135, $MgCl_2$ 2, EGTA 1, Na_2ATP 2, HEPES 10, pH 7.3 (adjusted with NaOH). The pipette was connected to the headstage of a patch clamp amplifier Axopatch-1D (Axon Instruments, Inc., Foster City, CA, USA), data were digitally sampled by Digidata 1200 (Axon Instruments, Inc.), and analysed by pCLAMP 10 software (Molecular Devices, Sunnyvale, CA, USA).

Statistics and calculations

Data are expressed as means ± SEM. Normalized dose–response curves were fitted by a modified Hill equation of the form $y = \alpha/[1 + (c/K_{1/2})^n] + (1 - \alpha)$, where c is the concentration; $K_{1/2}$ is the concentration at which half-maximal inhibition occurs; n is the Hill coefficient; and α is the fraction inhibited by the treatment. Statistical significance was estimated by Student's *t*-test for independent samples, one-way ANOVA followed by Scheffe's *post hoc* test or Pearson's product–moment correlation analysis (as indicated in the figure legends). The difference was considered to be significant at $P < 0.05$.

Results

Characterization of the RR sensitivity of K_{2P} channels: TREK-2 is potently inhibited by the polycationic compound

Different K_{2P} channel types were expressed in *Xenopus laevis* oocytes, and their sensitivity to the polycationic dye RR

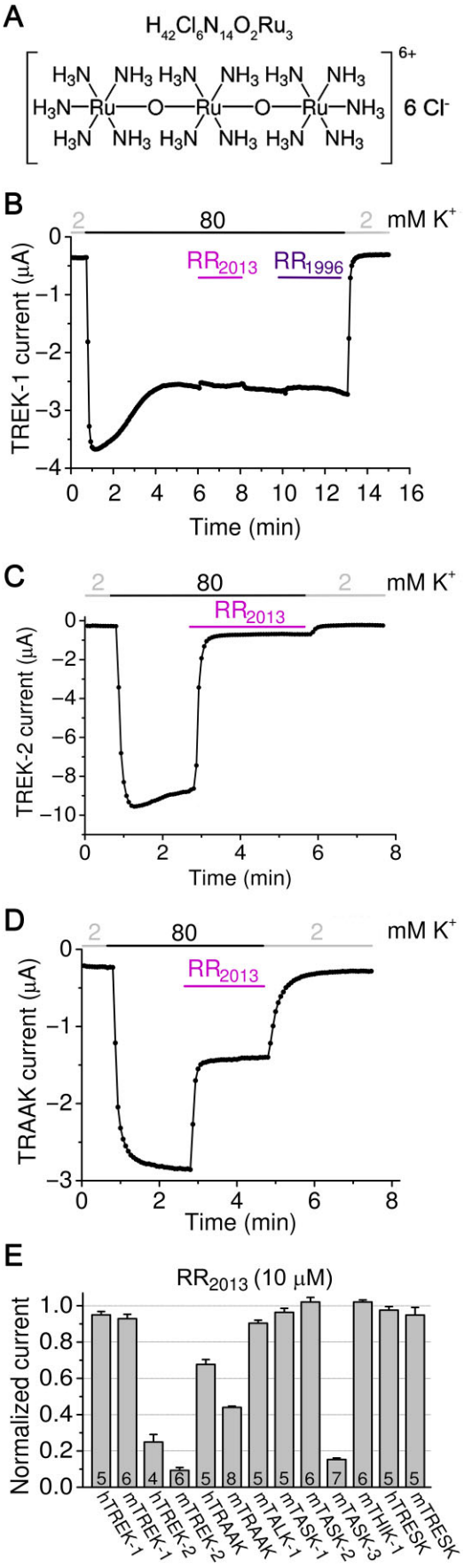

Figure 1

TREK-2, TRAAK and TASK-3 are blocked by RR. (A) Chemical structure and molecular formula of RR. (B) Representative two-electrode voltage clamp recording from a *Xenopus* oocyte expressing mouse TREK-1. After the rundown of TREK-1 current at the beginning of the measurement, two RR preparations were administered (RR_{2013} and RR_{1996} from Sigma, as indicated by the coloured horizontal bars). TREK-1 was not affected by RR (10 μM). The current was measured at –100 mV and the extracellular [K^+] was changed from 2 to 80 mM and back as shown above the recording. (C) The sensitivity of mouse TREK-2 channel to RR_{2013} was tested as in panel A. RR (10 μM) strongly inhibited TREK-2 current. (D) Representative recording of mouse TRAAK current inhibition by RR_{2013} (10 μM). The inhibition of TRAAK was intermediate between TREK-1 and TREK-2. (E) RR sensitivity of K2P channels (as indicated below the column graph) is illustrated. In addition to the positive control mouse TASK-3 (mTASK-3), human and mouse TREK-2 (hTREK-2 and mTREK-2) currents were also diminished by RR, whereas human and mouse TRAAK currents were less inhibited. TREK-1, TALK-1, TASK-1, TASK-2, THIK-1 and TRESK were not affected by RR [Where not specified otherwise, RR_{2013} of high purity was used in the experiments. All oocyte measurements were performed at room temperature (21°C).].

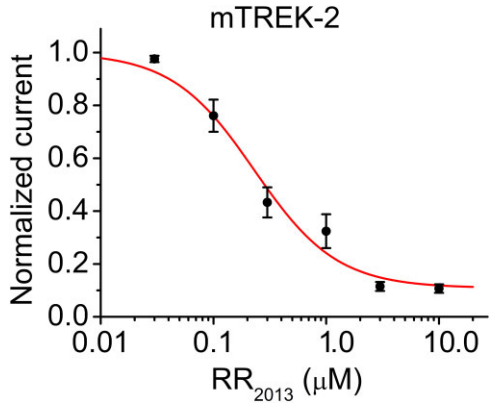

Figure 2

Dose–response relationship of TREK-2 current and RR concentration. Mouse TREK-2 currents were measured in high (80 mM) [K^+] at –100 mV in the presence of different (0.03, 0.1, 0.3, 1.0, 3.0 and 10.0 μM) concentrations of RR. The currents were corrected for the small non-specific leak in 2 mM extracellular [K^+] and normalized to the value without the inhibitor. Each data point represents the average of normalized currents of six to nine oocytes. The data points were fitted by a modified Hill equation (see Methods).

(Figure 1A) was measured at –100 mV in 80 mM [K^+] by two-electrode voltage clamp. In accordance with our previous results (Czirják and Enyedi, 2002a), human and mouse TREK-1 ($K_{2P}2.1$) currents were negligibly affected by the application of 10 μM RR (for representative recording, see Figure 1B). Neither of our RR preparations, purchased from Sigma in 1996 and 2013, respectively, were effective inhibitors of TREK-1. RR_{2013} reduced human TREK-1 currents by only 5.0 ± 1.9% ($n = 5$), and the mouse channel current by 7.1 ± 2.4% ($n = 6$; see *hTREK-1* and *mTREK-1* in Figure 1E). Unexpectedly, human and mouse TREK-2 ($K_{2P}10.1$) currents were substantially blocked by RR, despite the high amino acid

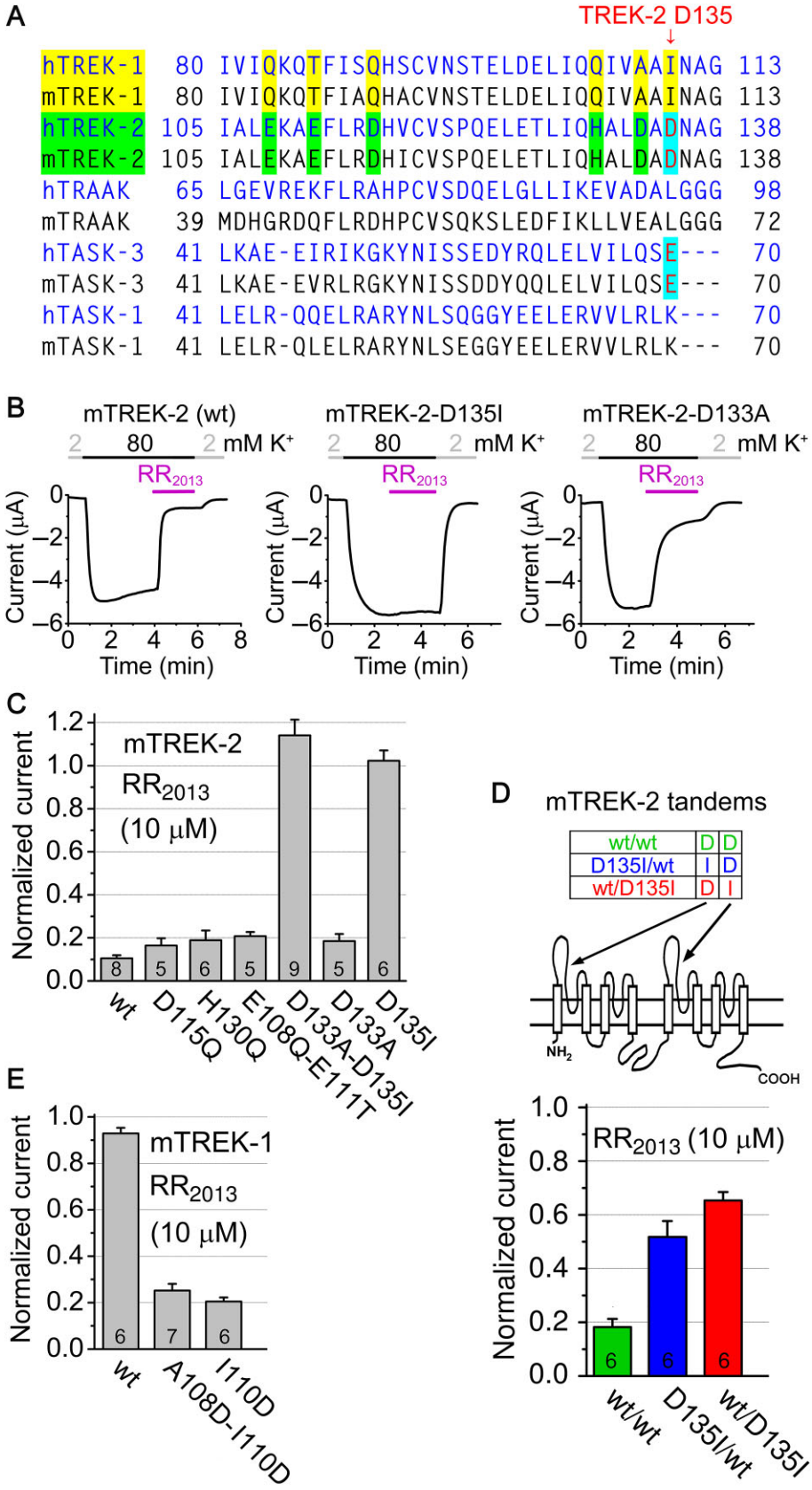
A
TREK-2 D135
hTREK-1 80 IVIQKQTFISQHSCVNSTELDELIQQIVAAINAG 113
mTREK-1 80 IVIQKQTFIAQHACVNSTELDELIQQIVAAINAG 113
hTREK-2 105 IALEKAEFLRDHVCVSPQELETLIQHALDADNAG 138
mTREK-2 105 IALEKAEFLRDHICVSPQELETLIQHALDADNAG 138
hTRAAK 65 LGEVREKFLRAHPCVSDQELGLLIKEVADALGGG 98
mTRAAK 39 MDHGRDQFLRDHPCVSQKSLEDFIKLLVEALGGG 72
hTASK-3 41 LKAE-EIRIKGKYNISSEDYRQLELVILQSE--- 70
mTASK-3 41 LKAE-EVRLRGKYNISSDDYQQLELVILQSE--- 70
hTASK-1 41 LELR-QQELRARYNLSQGGYEELERVVLRLK--- 70
mTASK-1 41 LELR-QLELRARYNLSEGGYEELERVVLRLK--- 70
B
mTREK-2 (wt)
mTREK-2-D135I
mTREK-2-D133A
2 80 2 mM K+
RR2013
Current (μA)
Time (min)
C
Normalized current
mTREK-2
RR2013
(10 μM)
wt
D115Q
H130Q
E108Q-E111T
D133A
D133A-D135I
D135I
D
mTREK-2 tandems
wt/wt
D135I/wt
wt/D135I
NH2
COOH
RR2013 (10 μM)
E
mTREK-1
RR2013
(10 μM)
wt
A108D-I110D
I110D

Figure 3

Mutation of aspartate 135 (D135) to isoleucine eliminates RR sensitivity of TREK-2, whereas the substitution of isoleucin 110 (I110) in TREK-1 with aspartate confers RR sensitivity to the channel. (A) Sequence alignment of a region of different K_{2P} channels (as indicated on the left) between the first transmembrane segment and the first pore domain. In this region, TREK-2 contains additional negatively charged or histidine residues, compared with TREK-1 (as indicated with yellow and green). D135 residue of TREK-2, corresponding to the RR-binding E70 amino acid of TASK-3, is indicated with red and cyan. (B) Representative recordings of mouse wild type (*wt*), D135I and D133A mutant TREK-2 currents and their sensitivity to RR were measured similarly as in panel C of Figure 1. (C) Sensitivity of wild type (*wt*) and different mutant versions of mouse TREK-2 (as indicated below the column diagram) to RR (10 μM). Negatively charged and histidine amino acids of TREK-2 were replaced by the corresponding (non-conserved) residues of the RR-resistant TREK-1. The current in the presence of RR was normalized to the initial value without the inhibitor. D133A-D135I double and D135I point mutations completely prevented the inhibition of TREK-2 by RR (ANOVA, Scheffe's *post hoc* test, $P < 10^{-5}$). The effect of the other mutations was not significant (The numbers in the columns indicate the number of oocytes measured.). (D) The two subunits of TREK-2 dimer were expressed as a tandem construct (consisting of a single polypeptide chain), as indicated in the scheme illustrating transmembrane topology. Mutation of D135 in the upstream (D135I/*wt*, blue) or downstream (*wt*/D135I, red) TREK-2 coding sequence reduced the inhibition by RR compared with the construct composed of the wild-type sequences (*wt*/*wt*, green, $P < 0.001$). (E) Normalized currents of wild-type (*wt*), A108D-I110D double and I110D point mutant TREK-1 in the presence of RR (10 μM).

sequence similarity of TREK-1 and TREK-2 channels (for representative recording see Figure 1C). Human TREK-2 was inhibited by 75.1 ± 4.2% (n = 4), whereas its mouse counterpart by 90.7 ± 1.6% (n = 6; see *hTREK-2* and *mTREK-2* in Figure 1E). RR_{1996} similarly inhibited TREK-2 as RR_{2013} (not shown). These data indicate that in addition to its discriminating effect on TASK channels, RR also distinguishes between the closely related TREK-1 and TREK-2 members of the K_{2P} family.

The third member of the TREK subfamily, TRAAK (K_{2P}4.1), was less inhibited by 10 μM RR_{2013} than TREK-2 (for representative recording see Figure 1D; 32.3 ± 2.7% (n = 5) and 56.0 ± 0.7% (n = 8) inhibition for human and mouse TRAAK, respectively, Figure 1E). This relatively weak inhibition of TRAAK by RR was not anticipated, because of our own previously reported data about the high sensitivity of the channel to RR (Czirják and Enyedi, 2002a), and urged us to investigate the reason for the apparent discrepancy between the present and previous data (see later). Among the other K_{2P} channels tested, mouse TASK-3 was inhibited (Figure 1E) as reported previously (Czirják and Enyedi, 2003), whereas mTALK-1, mTASK-1, mTASK-2, mTHIK-1 and mTRESK (and hTRESK) were not sensitive to the polycation (less than 10% inhibition, Figure 1E).

Aspartate 135 (D135) in the extracellular ion pathway (EIP) of TREK-2 is responsible for the inhibition by RR

As the RR sensitivity of TREK-2 is reported for the first time, we analysed this inhibitory effect in more detail. RR inhibited TREK-2 with a half-maximal inhibitory concentration of 0.23 ± 0.06 μM (Figure 2). Hill coefficient was 1.2 ± 0.3, suggesting that a single RR molecule interacted with the functional dimer. The rapid onset of the inhibition (Figure 1C) suggested that the RR-binding site of TREK-2 is extracellular, in good accordance with the limited permeation of the polycationic compound through the plasma membrane.

In order to identify the amino acids interacting with the RR molecule, we mutated negatively charged and histidine residues of TREK-2 in the first extracellular loop, where the sequence of TREK-2 differed from the RR-resistant TREK-1 (Figure 3A). We changed these amino acids in combinations or one-by-one to the corresponding residues of TREK-1, and tested the sensitivity of the constructs to 10 μM RR (Figure 3B and C). D115Q, H130Q and E108Q-E111T double mutants were inhibited by RR, similarly to the wild-type channel. In sharp contrast, the D133A-D135I double mutant was resistant to the inhibitor [mouse TREK-2c was used (Mirkovic and Wickman, 2011); the ALDADNA sequence is also conserved in other splice variants.]. Next, we examined the individual contribution of D133 and D135 to the inhibitory effect. The D133A construct was similarly sensitive to RR as the wild-type channel, but RR did not inhibit the D135I mutant (Figure 3B and C). Thus, D135 is the major determinant of the inhibition of TREK-2 by RR.

As K_{2P} channels function as dimers, we examined whether D135 of both subunits were necessary for the inhibition. We designed a tandem (concatenated) construct and expressed the two TREK-2 subunits as a continuous polypeptide (Figure 3D). Tandem TREK-2 was similarly sensitive to RR as the wild-type channel (81.8 ± 3.1% inhibition, n = 6, Figure 3D). Mutation of D135 in the N- or C-terminal half of the tandem construct reduced the sensitivity to RR (34.7 ± 3.1% (n = 6) and 48.2 ± 5.9% (n = 6) inhibition for *wt/D135I* and *D135I/wt* channels by 10 μM RR, respectively, Figure 3D). Thus, the D135 residues of both subunits contribute to the effect, although one intact D135 still allowed the inhibition by RR to some extent.

As discussed earlier, TREK-1 is resistant to RR (Figure 1B and E). Because TREK-1 has isoleucine (I110) in the position corresponding to D135 of TREK-2, we replaced this hydrophobic residue with the acidic aspartate. As opposed to the wild-type channel, the I110D point mutant of TREK-1 was substantially inhibited by 10 μM RR (79.5 ± 1.7% inhibition (n = 6); Figure 3E). The introduction of the aspartate to the appropriate position was sufficient to create an RR-binding site even in the molecular context of TREK-1.

RV inhibits TRAAK more potently than RR

Mouse TRAAK appeared to be less inhibited by RR in this study than we previously reported (Czirják and Enyedi, 2002a). An old commercial preparation of RR (Sigma 1996) evoked qualitatively different effect on TRAAK from that of our present RR batch (Sigma, 2013, Figure 4). In addition to the higher efficacy of RR_{1996}, the old product also inhibited TRAAK with slower kinetics than the new one. Mouse TRAAK was more efficiently inhibited by both RR preparations than

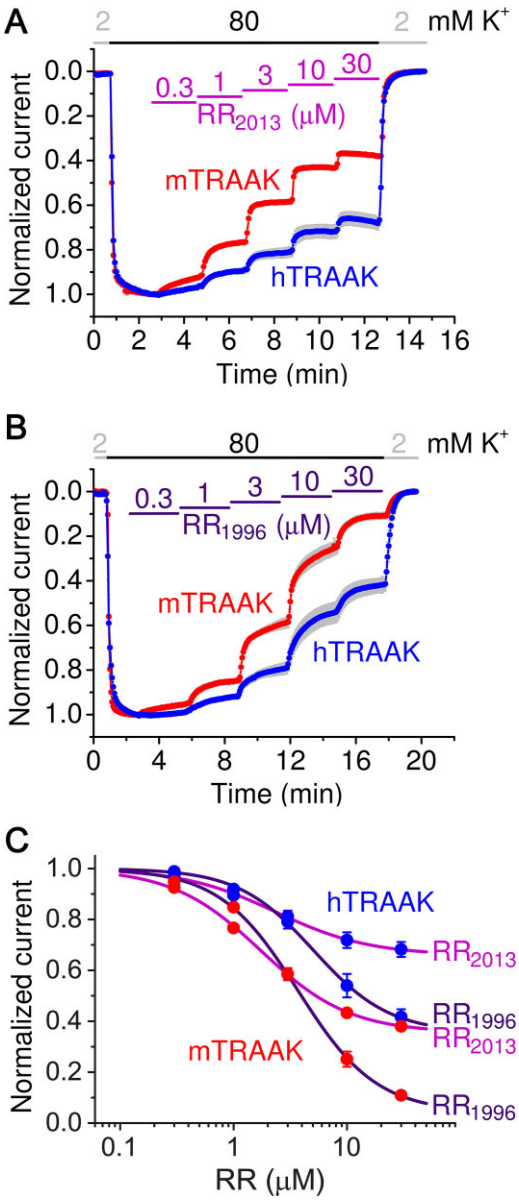

Figure 4

Inhibition of TRAAK by different commercial preparations of RR. (A) Normalized currents of human and mouse TRAAK are plotted in the presence of different concentrations of RR purchased from Sigma in 2013. (B) Similar measurement with an old RR preparation (Sigma 1996). Note the strong inhibition developing with slow kinetics. (C) Dose–response relationships of TRAAK current [human (*hTRAAK*) or mouse (*mTRAAK*)] and RR concentration (RR_{1996} or RR_{2013}, as indicated on the right) was calculated from the measurements in panels A and B, and fitted with the modified Hill equation (see Methods).

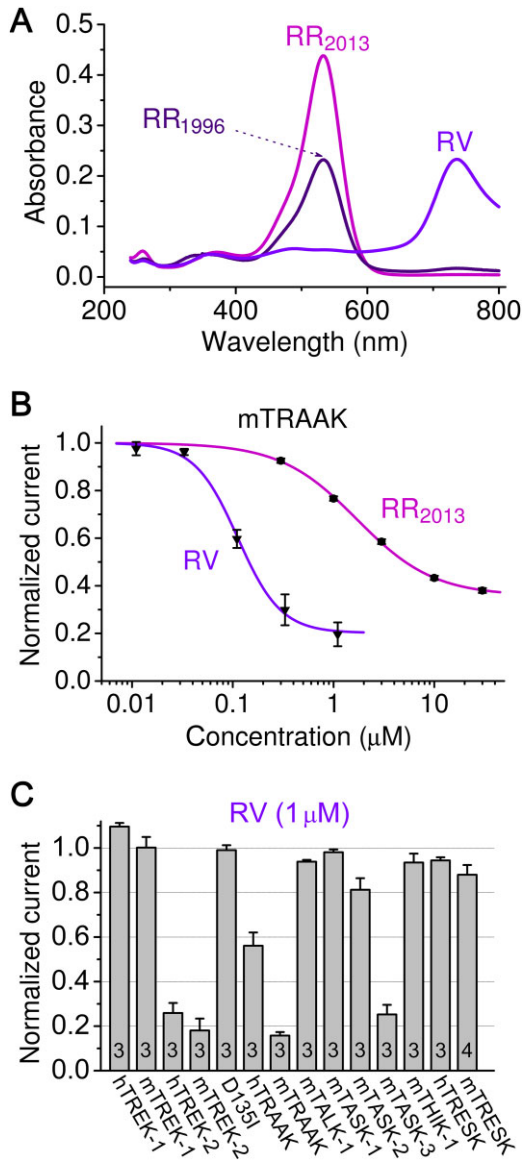

Figure 5

RV inhibits TRAAK more potently than RR. (A) Absorption spectra of equal mass (w/v) concentration of RR purchased from Sigma in 1996 (RR_{1996}) or in 2013 (RR_{2013}), and our purified RV preparation (RV). (B) Dose–response relationship of mouse TRAAK current and $RR_{(2013)}$ or RV. (C) Sensitivity of different K_{2P} channels (as indicated below the columns) to RV (1 μM) was measured. TASK-3, TREK-2 and mouse TRAAK were strongly inhibited. The D135I mutation of TREK-2 (D135I column) completely eliminated the sensitivity to RV.

the human orthologue; however, the slow kinetics of inhibition by RR_{1996} was apparent irrespective of the species (Figure 4).

It is known that commercial preparations of RR may contain contaminants, for example ruthenium ammine compounds (with absorption maxima between 200 and 400 nm), and RV (absorption peaks at 734 and 900 nm, see Luft, 1971). In the absorption spectra of equal mass concentration of RR_{1996} and RR_{2013}, the peak amplitudes at 533 nm, characteristic for RR, were different (Figure 5A). RR_{1996} preparation contained less RR than RR_{2013}, despite of the more pronounced inhibition of TRAAK by the older preparation. Therefore, we concluded that contaminants in the RR_{1996} sample also inhibit TRAAK in addition to RR (Where not specified otherwise, RR_{2013} of high purity was used throughout this study.).

As a small absorption peak at 734 nm was present in RR_{1996}, but not in RR_{2013} (Figure 5A), we examined whether RV ($[Ru_3N_2(NH_3)_8(OH)(OH_2)_5]Cl_5$) inhibits TRAAK (Hall and

Griffith, 1980). To this end, we purified RV by ion exchange chromatography using a low-charge density CM cellulose column (see Methods, and Figure 5A for the spectrum of purified RV). RV inhibited TRAAK with higher potency than RR (IC_{50} value of 0.11 ± 0.01 and 1.7 ± 0.1 μM for RV and $RR_{(2013)}$, respectively, Figure 5B). Hill coefficients for RR and RV were 1.1 ± 0.1 and 2.0 ± 0.3, respectively, suggesting that the mechanisms of action of the two ruthenium compounds on TRAAK are different. TRAAK dimer may contain two binding sites for RV, but only one for RR. Reconstitution of the absorption maxima of RR_{1996} at 533 and 734 nm by mixing RR_{2013} with purified RV indicated that RV was partly responsible for the difference of inhibition of mTRAAK by the two RR preparations (see Supporting Information). Our results suggest that RV is a more potent inhibitor of TRAAK than RR, and the effect of some commercial preparations of RR may also depend on their RV contamination in addition to their RR content.

The effect of RV was also tested on a more extensive set of K2P channels (Figure 5C). The inhibitory profiles of RR (Figure 1E) and RV (Figure 5C) turned out to be similar. The D135I mutation also prevented the inhibitory effect of RV (Figure 5C), suggesting a common site of action of RR and RV in the case of TREK-2 channel.

RR-sensitive background potassium current in DRG neurons

DRG neurons have been reported to express predominantly TREK-2 and the RR-insensitive TREK-1 and TRESK background K^+ channels in rodents (Talley *et al.*, 2001; Kang and Kim, 2006; Dobler *et al.*, 2007). We performed whole-cell patch clamp recordings on mouse DRG neurons at 37°C to investigate the RR-sensitive and temperature-dependent TREK-2 current (Kang *et al.*, 2005; Pereira *et al.*, 2014). In a representative neuron, RR (10 μM) inhibited the K^+ current by 71% at –100 mV in 30 mM extracellular [K^+], and the outward current was also reduced at positive potentials in accordance with the leak characteristics of the blocked current component (Figure 6A–C; voltage-gated K^+ channels dominated the outward current). High sensitivity to RR is compatible with the predominant contribution of TREK-2 to the background potassium current in this neuron [The reversal potential of the difference current (Figure 6B) closely approximates the calculated equilibrium potential of K^+ (–40 mV in 30 mM [K^+] at 37°C).]. RR also inhibited a small voltage-dependent component (between –60 and –40 mV), the ion selectivity of which has not been further examined. The saturation effect of the difference in current above +20 mV may be related to the voltage-dependent nature of the inhibition by the cationic dye.]

We examined the RR sensitivity of the K^+ currents of 20 DRG neurons with diameters ranging from 16 to 45 μm. The amplitudes of the K^+ currents (the differences of inward currents in 2 and 30 mM extracellular [K^+] at –100 mV) were between 120 and 2540 pA. The effect of RR varied considerably in this cell population, from complete insensitivity to about 75% inhibition (Figure 6D). We found weak negative correlation between the K^+ current amplitude and the RR sensitivity (r = –0.6, P < 0.005), suggesting that neurons with large K^+ current at –100 mV expressed relatively less TREK-2.

Discussion

K_{2P} background K^+ channels are the major determinants and regulators of the resting membrane potential in several cell types (Enyedi and Czirják, 2010). However, the pharmacological separation of their almost identical macroscopic currents has not yet been adequately resolved. In the absence of specific inhibitors, the pharmacological tools aiding the discrimination of the currents of different K_{2P} channels are appreciated. This explains that the otherwise relatively non-specific RR has been extensively used to distinguish between TASK-1 and TASK-3 currents.

In the present study, we demonstrate that RR also discriminates between TREK-1 and TREK-2 channels. In fact, this finding is so counter-intuitive that in a recent report, the RR insensitivity of TREK-2 has been anticipated because TREK-1 is not affected by the compound (Cadaveira-Mosquera *et al.*, 2011). However, RR can distinguish between target proteins depending on a single amino acid difference (per subunit), and such a decisive variation of sequence is present not only in the TASK channels, but also in the two closely related members of the TREK subfamily. The negatively charged aspartate 135 mediates the inhibition of TREK-2 by RR, in sharp contrast to the RR-resistant TREK-1, containing the hydrophobic isoleucine 110 in the corresponding position.

The outer entrance of the ion-conducting pore of K_{2P} channels is covered by an extracellular cap domain, as recently revealed by the crystal structures of TWIK-1 (PDB ID: 3UKM; Miller and Long, 2012), TRAAK (PDB ID: 3UM7 and 4I9W; Brohawn *et al.*, 2012; 2013) and TREK-2 (PDB ID: 4BW5). A short tunnel piercing through the extracellular cap, roughly parallel to the plane of the plasma membrane, the so-called EIP connects the extracellular space to the pore entrance (The EIP and the pore together form a T shape, where the horizontal line of the 'T' is the EIP, whereas the vertical line corresponds to the pore through the plasma membrane.). D135 residues are located in the middle of the EIP, on the ceiling of the tunnel, just above the selectivity filter, in symmetrical arrangement (Figure 7). We propose that this junction region between the EIP and the pore entrance is the binding site of RR, where the inhibitor can electrostatically and/or sterically hinder the movement of the charge carrier. D135 residue, identified in the present study, is located at a position of the EIP that is similar, or maybe even, identical to E70 of TASK-3 (Czirják and Enyedi, 2003; Gonzalez *et al.*, 2013). The exact position of D135 of TREK-2 and E70 of TASK-3 relative to the EIP appears to be slightly different (compare Figure 7 with Figure 1 in Gonzalez *et al.*, 2013); however, it remains a question how faithfully the static structure distorted into a protein crystal represents the fine details of side chain arrangements in the functional channels. The conditions of crystallization may have drastic effects on the conformation of K_{2P} channels as exemplified by the different reported structures of TRAAK (Brohawn *et al.*, 2012; 2013).

TREK channels are regulated in a highly complex manner, and most of the regulatory properties are shared by TREK-1 and TREK-2. Both channels are mechanosensitive, temperature-dependent, activated by intracellular acidification, volatile anaesthetics and polyunsaturated fatty acids,

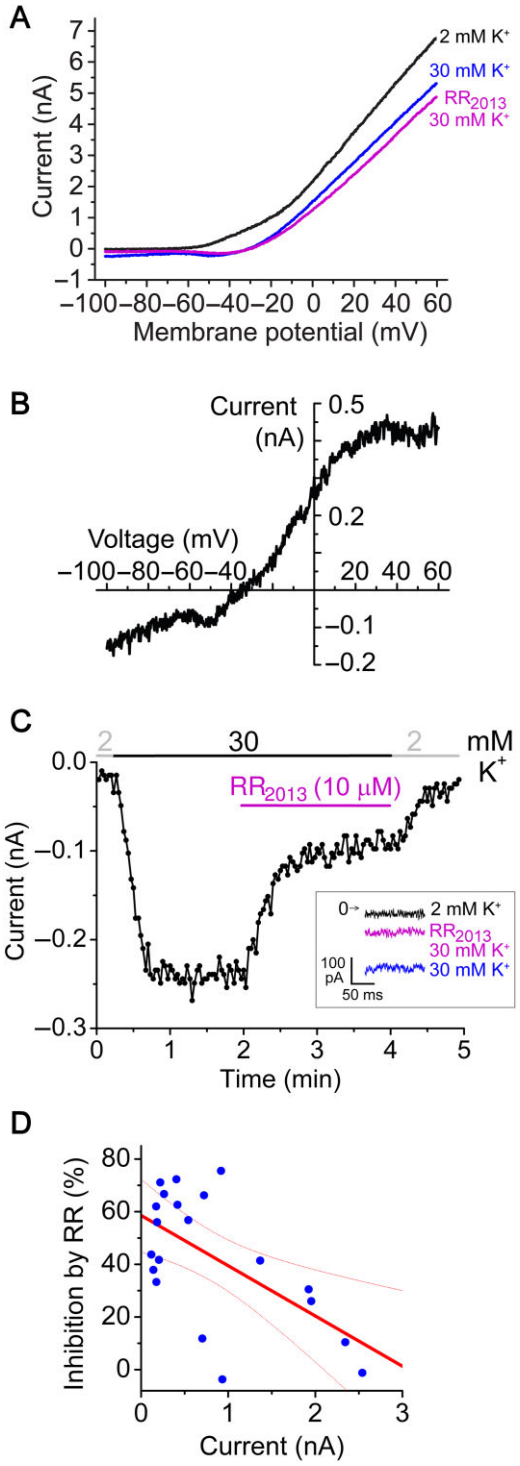

Figure 6

RR-sensitive background potassium current in DRG neurons. (A). Representative current–voltage (I–V) relationships from a mouse DRG neuron. Currents were measured in 2 mM or 30 mM extracellular [K^+] in the absence or presence of RR (10 μM) using a voltage protocol consisting of a step to –100 mV for 200 ms from a holding potential of –80 mV, followed by a 600 ms ramp to +60 mV. The I–V relationships were plotted from the ramp data. (B) The difference current inhibited by RR in the presence of 30 mM [K^+] is calculated from the data shown in panel A (by subtracting the magenta curve from the blue one). (C) Currents at –100 mV of the same DRG neuron as in panel A were plotted as a function of time. The currents measured during the voltage step to –100 mV are shown in the inset. (D) Correlation between the K^+ current amplitude and the RR sensitivity for 20 DRG neurons. The regression line (red solid) and 95% confidence band (red dotted curves) of Pearson's correlation analysis are indicated. All DRG measurements were performed at 37°C.

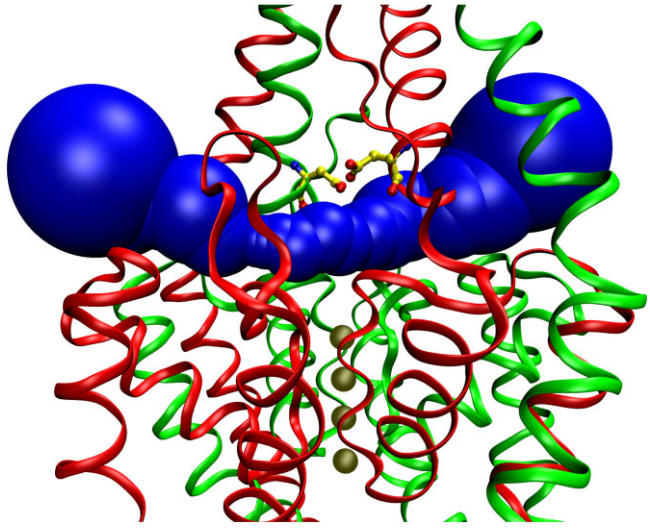

Figure 7

Aspartate 135 residues are positioned in the EIP above the selectivity filter. The EIP tunnel is filled with a series of blue spheres in this schematic representation of human TREK-2 crystal structure (PDB ID: 4BW5, A. C. W. Pike, *et al.*, unpublished). K^+ ions in the vertical channel pore are illustrated with four solid (tan) spheres below the EIP. Aspartate 135 (D135) residues (yellow ball and stick representation, with red oxygen and blue nitrogen atoms) are located on the ceiling of the EIP above the selectivity filter. The two subunits are drawn as red and green ribbons. The view is not exactly perpendicular to the direction of the EIP, but the structure is slightly rotated around the vertical axis, in order to avoid the overlap of the D135 residues of the two subunits. The NSSN and NSSNNS sequences of the subunits, respectively, are not resolved by the crystal structure; however, this does not affect the EIP. The graphics were produced with MolAxis (Yaffe *et al.*, 2008) and VMD (Humphrey *et al.*, 1996) software.

and inhibited by PKA, PKC and AMP-activated protein kinase (Enyedi and Czirják, 2010). Although most properties of TREK-1 and TREK-2 are identical, some differences between them have also been reported. Extracellular acidification inhibits TREK-1, but activates TREK-2, depending on the protonation of a conserved histidine residue in the first extracellular loop of the channels (Sandoz *et al.*, 2009; Bagriantsev *et al.*, 2011). The two TREK channels can also be distinguished on the basis of their different single-channel conductance; however, this approach is complicated by the multiple conductance levels arising from alternative translation initiation variants (Simkin *et al.*, 2008; Thomas *et al.*, 2008). TREK-1 and TREK-2 are differentially expressed in the CNS and also at the periphery, suggesting that the two apparently similar channel types may have different functions (for review, see Noel *et al.*, 2011). RR distinguishes between the

macroscopic currents of TREK-1 and TREK-2, and may complement the presently available methodological repertoire for the discrimination of the two channel types.

RR also inhibits the third member of the TREK subfamily, TRAAK, although less efficiently than we originally reported (Czirják and Enyedi, 2002a). Despite of its lower pure RR content, RR_{1996} preparation was a more effective inhibitor of TRAAK than RR_{2013}. RV also contributed to the inhibition of TRAAK by the old preparation. The different Hill coefficients for RR and RV suggest that not only their affinities to TRAAK, but also the mechanisms of action of the two ruthenium compounds are different. It is probable that RR and RV also inhibit TRAAK by binding to negatively charged extracellular regions of the channel; however, the identification of these binding sites is not straightforward. Mouse TRAAK subunit contains 14 negatively charged (Asp and Glu) and 5 histidine (His) residues in its extracellular loops. The sequence alignments of TRAAK with the TREK channels and the crystal structures are not particularly helpful for the prediction of the regions responsible for the interaction. Therefore a comprehensive mutational screening approach will be required in the future to determine which amino acids constitute the RR and RV binding sites of TRAAK.

DRG neurons express several K_{2P} channel types, as detected by *in situ* hybridization (Talley *et al.*, 2001). The contribution of different channels to the ensemble background K^+ current was estimated by single-channel analysis (Kang and Kim, 2006). TREK-2 was suggested to contribute 69% to the background K^+ current at 37°C, followed by TRESK (16%), TREK-1 (12%), and TRAAK (3%). In a recent report, TREK-2 was immunodetected in a high number of DRG neurons, and small DRG neurons were found to contain higher TREK-2 immunoreactivity than the large cells (Acosta *et al.*, 2014).

We were curious whether we can detect the RR-sensitive TREK-2 current component by whole-cell patch clamp measurements in isolated DRG neurons. In several cells, characterized by relatively small (<0.5 nA) K^+ current amplitudes at –100 mV in high (30 mM) $[K^+]$, RR inhibited the current by 60–70%. This strong inhibition by RR is consistent with high TREK-2 expression, and is in good accordance with the previous immunocytochemistry data that small cells express TREK-2 most abundantly (Acosta *et al.*, 2014). Evidently, TRAAK and TASK-3 may have also contributed to the current inhibited by RR, although previous reports suggest that TREK-2 is predominant. On the other hand, in some neurons, characterized by relatively large (>0.5 nA) K^+ current amplitudes, the background potassium current was weakly (<20%) inhibited by RR, indicating that in these cells TREK-2 (as well as TRAAK and TASK-3) were minor components. In summary, we provided the first data about the contribution of TREK-2 to the whole-cell background potassium current of individual DRG neurons, and our results suggest that RR can also be applied for the verification of TREK-2 current in other native cell types.

Acknowledgements

This work was supported by the Hungarian National Research Fund (OTKA K108496). The skilful technical assistance of Alice Dobolyi and Irén Veres is acknowledged.

Author contributions

All authors conceived, designed, and performed the experiments; analysed the data and wrote the paper.

Conflict of interest

None.

References

Acosta C, Djouhri L, Watkins R, Berry C, Bromage K, Lawson SN (2014). TREK2 expressed selectively in IB4-binding C-fiber nociceptors hyperpolarizes their membrane potentials and limits spontaneous pain. J Neurosci 34: 1494–1509.

Alexander SPH, Benson HE, Faccenda E, Pawson AJ, Sharman JL, Spedding M *et al.* (2013). The Concise Guide to PHARMACOLOGY 2013/14: Ion channels. Br J Pharmacol 170: 1607–1651.

Aller MI, Veale EL, Linden AM, Sandu C, Schwaninger M, Evans LJ *et al.* (2005). Modifying the subunit composition of TASK channels alters the modulation of a leak conductance in cerebellar granule neurons. J Neurosci 25: 11455–11467.

Bagriantsev SN, Peyronnet R, Clark KA, Honore E, Minor DL Jr (2011). Multiple modalities converge on a common gate to control K2P channel function. EMBO J 30: 3594–3606.

Berg AP, Bayliss DA (2007). Striatal cholinergic interneurons express a receptor-insensitive homomeric TASK-3-like background K^+ current. J Neurophysiol 97: 1546–1552.

Berg AP, Talley EM, Manger JP, Bayliss DA (2004). Motoneurons express heteromeric TWIK-related acid-sensitive K^+ (TASK) channels containing TASK-1 (KCNK3) and TASK-3 (KCNK9) subunits. J Neurosci 24: 6693–6702.

Bittner S, Budde T, Wiendl H, Meuth SG (2010). From the background to the spotlight: TASK channels in pathological conditions. Brain Pathol 20: 999–1009.

Brohawn SG, del Marmol J, MacKinnon R (2012). Crystal structure of the human K2P TRAAK, a lipid- and mechano-sensitive K^+ ion channel. Science 335: 436–441.

Brohawn SG, Campbell EB, MacKinnon R (2013). Domain-swapped chain connectivity and gated membrane access in a Fab-mediated crystal of the human TRAAK K^+ channel. Proc Natl Acad Sci U S A 110: 2129–2134.

Cadaveira-Mosquera A, Ribeiro SJ, Reboreda A, Perez M, Lamas JA (2011). Activation of TREK currents by the neuroprotective agent riluzole in mouse sympathetic neurons. J Neurosci 31: 1375–1385.

Czirják G, Enyedi P (2002a). Formation of functional heterodimers between the TASK-1 and TASK-3 two-pore domain potassium channel subunits. J Biol Chem 277: 5426–5432.

Czirják G, Enyedi P (2002b). TASK-3 dominates the background potassium conductance in rat adrenal glomerulosa cells. Mol Endocrinol 16: 621–629.

Czirják G, Enyedi P (2003). Ruthenium red inhibits TASK-3 potassium channel by interconnecting glutamate 70 of the two subunits. Mol Pharmacol 63: 646–652.

Czirják G, Enyedi P (2006). Zinc and mercuric ions distinguish TRESK from the other two-pore-domain K^+ channels. Mol Pharmacol 69: 1024–1032.

Czirják G, Tóth ZE, Enyedi P (2004). The two-pore domain K^+ channel, TRESK, is activated by the cytoplasmic calcium signal through calcineurin. J Biol Chem 279: 18550–18558.

Deng PY, Lei S (2008). Serotonin increases GABA release in rat entorhinal cortex by inhibiting interneuron TASK-3 K^+ channels. Mol Cell Neurosci 39: 273–284.

Dobler T, Springauf A, Tovornik S, Weber M, Schmitt A, Sedlmeier R *et al.* (2007). TRESK two-pore-domain K^+ channels constitute a significant component of background potassium currents in murine dorsal root ganglion neurones. J Physiol 585: 867–879.

Enyedi P, Czirják G (2010). Molecular background of leak K^+ currents: two-pore domain potassium channels. Physiol Rev 90: 559–605.

Ernest NJ, Logsdon NJ, McFerrin MB, Sontheimer H, Spiller SE (2010). Biophysical properties of human medulloblastoma cells. J Membr Biol 237: 59–69.

Gonzalez W, Zuniga L, Cid LP, Arevalo B, Niemeyer MI, Sepulveda FV (2013). An extracellular ion pathway plays a central role in the cooperative gating of a K(2P) K^+ channel by extracellular pH. J Biol Chem 288: 5984–5991.

Hall JP, Griffith WP (1980). Studies on transition-metal nitrido- and oxo-complexes. Part 6. Nitrido-bridged complexes of osmium and ruthenium. J Chem Soc Dalton Trans 2410–2414.

Humphrey W, Dalke A, Schulten K (1996). VMD: visual molecular dynamics. J Mol Graph 14: 33–38.

Kang D, Kim D (2006). TREK-2 (K2P10.1) and TRESK (K2P18.1) are major background K^+ channels in dorsal root ganglion neurons. Am J Physiol Cell Physiol 291: C138–C146.

Kang D, Han J, Talley EM, Bayliss DA, Kim D (2004). Functional expression of TASK-1/TASK-3 heteromers in cerebellar granule cells. J Physiol 554: 64–77.

Kang D, Choe C, Kim D (2005). Thermosensitivity of the two-pore domain K^+ channels TREK-2 and TRAAK. J Physiol 564: 103–116.

Kilkenny C, Browne W, Cuthill IC, Emerson M, Altman DG (2010). Animal research: reporting *in vivo* experiments: the ARRIVE guidelines. Br J Pharmacol 160: 1577–1579.

Kim D, Cavanaugh EJ, Kim I, Carroll JL (2009). Heteromeric TASK-1/TASK-3 is the major oxygen-sensitive background K^+ channel in rat carotid body glomus cells. J Physiol 587: 2963–2975.

Larkman PM, Perkins EM (2005). A TASK-like pH- and amine-sensitive 'leak' K^+ conductance regulates neonatal rat facial motoneuron excitability in vitro. Eur J Neurosci 21: 679–691.

Lauritzen I, Zanzouri M, Honore E, Duprat F, Ehrengruber MU, Lazdunski M *et al.* (2003). K^+-dependent cerebellar granule neuron apoptosis. Role of task leak K^+ channels. J Biol Chem 278: 32068–32076.

Lotshaw DP (2007). Biophysical, pharmacological, and functional characteristics of cloned and native mammalian two-pore domain K^+ channels. Cell Biochem Biophys 47: 209–256.

Luft JH (1971). Ruthenium red and violet. I. Chemistry, purification, methods of use for electron microscopy and mechanism of action. Anat Rec 171: 347–368.

Mathie A, Veale EL (2007). Therapeutic potential of neuronal two-pore domain potassium-channel modulators. Curr Opin Investig Drugs 8: 555–562.

McGrath JC, Drummond GB, McLachlan EM, Kilkenny C, Wainwright CL (2010). Guidelines for reporting experiments involving animals: the ARRIVE guidelines. Br J Pharmacol 160: 1573–1576.

Miller AN, Long SB (2012). Crystal structure of the human two-pore domain potassium channel K2P1. Science 335: 432–436.

Mirkovic K, Wickman K (2011). Identification and characterization of alternative splice variants of the mouse Trek2/Kcnk10 gene. Neuroscience 194: 11–18.

Musset B, Meuth SG, Liu GX, Derst C, Wegner S, Pape HC *et al.* (2006). Effects of divalent cations and spermine on the K^+ channel TASK-3 and on the outward current in thalamic neurons. J Physiol 572: 639–657.

Noel J, Sandoz G, Lesage F (2011). Molecular regulations governing TREK and TRAAK channel functions. Channels (Austin) 5: 402–409.

Olschewski A, Li Y, Tang B, Hanze J, Eul B, Bohle RM *et al.* (2006). Impact of TASK-1 in human pulmonary artery smooth muscle cells. Circ Res 98: 1072–1080.

Pawson AJ, Sharman JL, Benson HE, Faccenda E, Alexander SP, Buneman OP *et al.*; NC-IUPHAR (2014). The IUPHAR/BPS Guide to PHARMACOLOGY: an expert-driven knowledgebase of drug targets and their ligands. Nucl Acids Res 42 (Database Issue): D1098–D1106.

Pereira V, Busserolles J, Christin M, Devilliers M, Poupon L, Legha W *et al.* (2014). Role of the TREK2 potassium channel in cold and warm thermosensation and in pain perception. Pain 155: 2534–2544.

Putzke C, Wemhoner K, Sachse FB, Rinne S, Schlichthorl G, Li XT *et al.* (2007). The acid-sensitive potassium channel TASK-1 in rat cardiac muscle. Cardiovasc Res 75: 59–68.

Sandoz G, Douguet D, Chatelain F, Lazdunski M, Lesage F (2009). Extracellular acidification exerts opposite actions on TREK1 and TREK2 potassium channels via a single conserved histidine residue. Proc Natl Acad Sci U S A 106: 14628–14633.

Simkin D, Cavanaugh EJ, Kim D (2008). Control of the single channel conductance of K2P10.1 (TREK-2) by the amino-terminus: role of alternative translation initiation. J Physiol 586: 5651–5663.

Talley EM, Solorzano G, Lei Q, Kim D, Bayliss DA (2001). Cns distribution of members of the two-pore-domain (KCNK) potassium channel family. J Neurosci 21: 7491–7505.

Thomas D, Plant LD, Wilkens CM, McCrossan ZA, Goldstein SA (2008). Alternative translation initiation in rat brain yields K2P2.1 potassium channels permeable to sodium. Neuron 58: 859–870.

Weber M, Schmitt A, Wischmeyer E, Doring F (2008). Excitability of pontine startle processing neurones is regulated by the two-pore-domain K^+ channel TASK-3 coupled to 5-HT2C receptors. Eur J Neurosci 28: 931–940.

Yaffe E, Fishelovitch D, Wolfson HJ, Halperin D, Nussinov R (2008). MolAxis: a server for identification of channels in macromolecules. Nucleic Acids Res 36: W210–W215.

Supporting information

Additional Supporting Information may be found in the online version of this article at the publisher's web-site:

http://dx.doi.org/10.1111/bph.13019

Figure S1 Ruthenium violet is partly responsible for the different effect of RR_{1996} and RR_{2013} on TRAAK.